Published in final edited form as:
J Nanopart Res. 2013 August 1; 15(8): 1874–. doi:10.1007/s11051-013-1874-0.

Effect of surface charge on the colloidal stability and in vitro uptake of carboxymethyl dextran-coated iron oxide nanoparticles

Vanessa Ayala,
Department of Chemical Engineering, University of Puerto Rico, PO Box 9000, Mayagüez, PR 00681, USA

Adriana P. Herrera,
Department of Chemical Engineering, University of Puerto Rico, PO Box 9000, Mayagü¨z, PR 00681, USA

Magda Latorre-Esteves,
Department of Chemical Engineering, University of Puerto Rico, PO Box 9000, Mayagüez, PR 00681, USA

Madeline Torres-Lugo, and
Department of Chemical Engineering, University of Puerto Rico, PO Box 9000, Mayagüez, PR 00681, USA

Carlos Rinaldi
Department of Chemical Engineering, University of Puerto Rico, PO Box 9000, Mayagüez, PR 00681, USA

Abstract

Nanoparticle physicochemical properties such as surface charge are considered to play an important role in cellular uptake and particle–cell interactions. In order to systematically evaluate the role of surface charge on the uptake of iron oxide nanoparticles, we prepared carboxymethyl-substituted dextrans with different degrees of substitution, ranging from 38 to 5 groups per chain, and reacted them using carbodiimide chemistry with amine–silane-coated iron oxide nanoparticles with narrow size distributions in the range of 33–45 nm. Surface charge of carboxymethyl-substituted dextran-coated nano-particles ranged from −50 to 5 mV as determined by zeta potential measurements, and was dependent on the number of carboxymethyl groups incorporated in the dextran chains. Nanoparticles were incubated with CaCo-2 human colon cancer cells. Nanoparticle–cell interactions were observed by confocal laser scanning microscopy and uptake was quantified by elemental analysis using inductively coupled plasma mass spectroscopy. Mechanisms of internalization were inferred using pharmacological inhibitors for fluid-phase, clathrin-mediated, and caveola-mediated endocytosis. Results showed increased uptake for nanoparticles with greater negative charge. Internalization patterns suggest that uptake of the most negatively charged particles occurs via non-specific interactions.

Correspondence to: Carlos Rinaldi.

Present Address: C. Rinaldi, J. Crayton Pruitt Family Department of Biomedical, Engineering, University of Florida, PO Box 116131, Gainesville, FL 32611-6131, USA. carlos.rinaldi@bme.ufl.edu

Electronic supplementary material: The online version of this article (doi:10.1007/s11051-013-1874-0) contains supplementary material, which is available to authorized users.

Keywords

Iron oxide; Dextran; Surface charge; Uptake; Endocytosis

Introduction

Colloidal dispersions of magnetic nanoparticles exhibit a unique combination of fluidity and capability to interact with external magnetic fields, which make them interesting for medical and biological applications. Factors such as magnetic structure, particle size, surface chemistry, and surface charge typically determine the magnetic response and physical or chemical interactions of the nanoparticles with biological entities during application. Emerging novel applications are focused on the development of magnetic nanoparticles as targeted magnetic carriers for drug delivery (Klostergaard and Seeney 2012; Gautier et al. 2012; Manju and Sreenivasan 2011; Chen et al. 2011; Veiseh et al. 2010), the usage of magnetic nanoparticles as specific contrast enhancement agents for in vivo magnetic resonance imaging (MRI) (Jung et al. 2011; Bhattacharya et al. 2011), protein immobilization (Huang et al. 2010; Li et al. 2010), magnetic cell sorting (Xu et al. 2011; Chen et al. 2011), and biocompatible magnetic nanoparticles for cancer treatment mediated by hyperthermia (Creixell et al. 2011; Mikhaylov and Vasiljeva 2011; Laurent et al. 2011; Arias et al. 2011).

In biomedical applications, magnetic nanoparticles are exposed to different pH and ionic strength conditions. For example, the pH inside tumor tissues is ∼6.8, while cellular compartments such as endosomes and lysosomes have a more acidic environment in a pH range of ∼4–5 (Modi et al. 2009; Cooper and Hausman 2009). Therefore, it is essential to obtain magnetic colloids that are stable against aggregation or precipitation in a wide range of pH. Such stability can be achieved through either electrostatic or steric repulsion forces. While steric repulsion forces depend on parameters such as molecular weight and graft density of the coating, electrostatic repulsion is affected by nanoparticle surface charge and ionic strength and pH of the solution (French et al. 2009). Thus, tuning nanoparticle surface charge may be one route to achieving colloidal stability, although the high ionic strength of biological media must be taken into consideration.

Surfactant- and polymer-based coatings have been tested for biocompatibility. The most common coatings are polysaccharides such as chitosan (Grenha 2012), starch (Cole et al. 2011), dextran (Chao et al. 2012), derivatives of dextran (Han et al. 2010), and other synthetic polymers such as polyethylene oxide (Phadatare et al. 2012; Häfeli et al. 2009). Among these, dextran has been shown to provide the required stability with no reported toxicity index (Ravikumar et al. 2012). In fact, dextran-coated iron oxide nanoparticles, marketed as Feridex IV.® and Ferumoxytol, have been approved by the U.S. Food and Drug Administration for use as contrast agents for MRI and iron deficiency anemia, respectively (de Chickera et al. 2011; Santosh et al. 2010). Carboxymethyl-substituted dextran (CMDx) is an anionic derivative of dextran commonly used as coating material for biosensors in both research and commercial settings due to its high density of carboxymethyl groups available for chemical conjugations (Ning et al. 2011). Additionally, CMDx had shown to be cleared more slowly from circulation than the unmodified form (Ning et al. 2011) and to exhibit low-fouling activity (Dubiel et al. 2012). Furthermore, the carboxymethyl groups allow for covalent fixation of the polymer to the particles' surface which has a favorable impact on the nanoparticles' colloidal stability (Creixell et al. 2010). Coating nanoparticles with polymers allows for colloidal stabilization through steric repulsion, which is less susceptible to the effects of high ionic strength of the biological medium. Nevertheless, the polymer coatings used sometimes possess charged groups (e.g., carboxylic or amine groups) in their

unmodified form, or a charged group is added to facilitate conjugation to the nanoparticles or to allow for subsequent modification with a reporter or targeting species.

Nanoparticle physicochemical properties such as surface charge and the chemical nature of the coating influence particle uptake, pharmacokinetics, and biodistribution (Bahmani et al. 2011; Jung et al. 2010; Georgieva et al. 2011; Alhareth et al. 2012; Arnida et al. 2011) ultimately affect the effectiveness of magnetic nanoparticles in medical treatments. Surface charge can also influence the pathway by which nanoparticles are internalized in cells, which in turn directs their intracellular fate and retention time (Gratton et al. 2008; Rauch et al. 2012). Finally, particle surface charge can promote nonspecific interactions with other molecules present in biological fluids, such as proteins, leading to their adsorption (Guarnieri et al. 2011), forming a layer known as a protein corona (Laurent et al. 2012). Since this protein corona remains in the particle surface long enough, what is actually interacting with the cell is the proteincoated nanoparticles and not the particle alone (Walczyk et al. 2010). The interactions of these protein particle systems with cells are also influenced by the "cell vision" effect, the first contact of the proteincoated particle with the cell membrane and is determined by the membrane composition of the "cell observer" (i.e., cell type) (Laurent et al. 2012). Specifically, it has been shown that particle toxicity and uptake depend on the "cell observer" (Laurent et al. 2013; Mahmoudi et al. 2012). Protein adsorption in turn modifies the surface charge and chemical nature of the nanoparticles, leading to often unexpected changes in their pharmacokinetics and biodistribution at the whole-animal level and their uptake and intracellular fate at the cellular level (Jedlovszky-Hajdú et al. 2012).

The potential impact of nanoparticle surface charge on their interactions with cells has motivated numerous studies on the uptake of iron oxide nanoparticles. In an early study, Wilhelm et al. (2003) compared the intracellular uptake of dextran-coated nanoparticles and anionic maghemite nanoparticles coated with meso-2,3-dimercaptosccinic acid (DMSA). The negatively charged DMSA-coated nanoparticles interacted non-specifically with the plasma membrane and were captured by HeLa cells with an efficiency three orders of magnitude higher than the neutral dextran-coated nanoparticles. Pradhan et al. (2007) compared uptake of lauric acid- and dextran-coated iron oxide nanoparticles in mouse fibroblast and human cervical carcinoma cell lines. Both coatings were adsorbed to the nanoparticle surface. The negatively charged lauric acid-coated nanoparticles not only had higher uptake than the dextran-coated nanoparticles, but also had higher cytotoxicity. Thorek and Tsourkas (2008) evaluated the effect of positive charge on uptake of iron oxide nanoparticles in non-phagocytic T-cells. Nanoparticles were coated by adsorption of dextran, followed by amination and crosslinking, and surface charge was tuned by blocking amine groups with glycidol. Nanoparticle uptake was observed to increase with the magnitude of positive surface charge. Osakaa et al. (2009) measured uptake of bare iron oxide nanoparticles with different surface charges in the breast cancer cell lines MCF-7 and HUVEC. The bare particles consisted of large (1–2 μm) aggregates of small (40 nm) particles and had either positive or negative charge, determined through synthesis conditions. Positively charged particles had higher uptake in MCF-7 cells whereas no charge dependence was observed in HUVEC cells. Ge et al. (2009) studied the effect of surface charge of iron oxide nanoparticles on uptake by oral squamous carcinoma cell KB. Negatively charged nanoparticles were obtained by adsorption of DMSA and positively charged nanoparticles were obtained by adsorption of chitosan through hydroxyl groups. Uptake was observed to depend on charge and incubation time, and positively charged nanoparticles had greater uptake than negatively charged nanoparticles for incubation times between 2 and 8 h. When incubated for 8 h no significant difference was observed in cellular uptake. Villanueva et al. (2009) compared uptake of iron oxide nanoparticles coated with dextran (neutral), amino-dextran (positive), heparin (negative), and DMSA (negative), in the

human cervical carcinoma cell line, HeLa. The various coatings were adsorbed to the nanoparticle surface. No internalization was observed for neutral particles. Negatively charged particles showed coating- and concentration-dependent uptake, where DMSA-coated nanoparticles showed lower uptake than heparin-coated nanoparticles. However, heparin-coated nanoparticles seemed to be cytotoxic. Positively charged nanoparticles had higher uptake than heparin-coated particles, without inducing cytotoxicity.

The studies cited above indicate that iron oxide nanoparticle surface charge has an important role in determining cellular uptake. However, these studies have suffered from a variety of limitations. First, in many of these studies nanoparticles with different surface charges were obtained by coating with different types of polymer or molecules, or by using bare nanoparticles. This resulted in nanoparticles with significantly different sizes and surface chemical nature, both of which may contribute to cellular uptake, obscuring the actual role of surface charge. Second, in many of these studies the colloidal stability of the nanoparticles under the conditions of the cellular uptake experiments was not demonstrated. Colloidal stability impacts the actual hydrodynamic diameter and shape of nanoparticles and can have a profound impact on extent and mechanism of uptake in cells. Furthermore, lack of colloidal stability during an uptake experiment may confound the role of surface charge on cellular uptake. For example, nanoparticles that are not stable may settle onto the membrane of fixed cells and be internalized irrespective of their surface charge, incorrectly indicating that charge has no influence on uptake. Third, in many of these studies particles were coated with polymers by adsorption. It has been recently demonstrated that polymers adsorbed onto iron oxide nanoparticle surfaces are rapidly displaced by species that are prevalent in biological fluids and cell culture media (Miles et al. 2008; Wotschadlo et al. 2009; Creixell et al. 2010). As such, there is the possibility that the surface charge, chemical nature, and colloidal stability of the nanoparticles used in many previous studies changed when put in contact with cells and their culture media, confounding the interpretation of the results. Thus, there is still a need for systematic studies of the effect of nanoparticle surface charge on their cellular uptake in which the physicochemical properties and colloidal stability of the nanoparticles are well documented. Here we report one such study, wherein we investigate the effect of the magnitude of negative surface charge (quantified by the zeta potential) on extent and mechanism of uptake of carboxymethyl dextran-coated nanoparticles in the colon cancer cell line CaCo-2.

Materials and methods

Materials

Iron (III) chloride hexahydrate 97 %, oleic acid, dextran, chloroacetic acid 99 %, 1-ethyl-3-(3-dimethylaminopropyl) carbodiimide hydrochloride (EDC), *N*-hydroxysuccinimide (NHS) 98 %, acetic acid 99.7 %, fluorescein-amine isomer I, Dulbecco's Modified Eagle's Medium (DMEM), Hank's balanced salt solution (HBSS), and phosphate buffered saline (PBS) were obtained from Sigma-Aldrich. 3-Aminopropyltriethoxysilane (APS) and sodium oleate were obtained from TCI America. 1-Octadecene was obtained from Alfa-Aesar. Hexane and anhydrous ethanol were obtained from Fisher Scientific. CaCo-2 cells were obtained from American Type Culture Collection. Fetal bovine serum (FBS) was obtained from Invitrogen. The fluorescent dye DiD and the nuclear stain DAPI were obtained from Molecular Probes. The endocytosis inhibitors 5-(*N*-ethyl-*N*-isopropyl) amiloride, dansylcadaverine, and filipin were obtained from Sigma-Aldrich. All materials were used as received.

Synthesis of magnetic nanoparticles coated with APS

Magnetic nanoparticles were synthesized by the thermal decomposition method using 1-octadecene as solvent (Park et al. 2004; Bao et al. 2007). An iron oleate solution was

prepared by mixing 6.4 g of the iron (III) salt and 24 g of sodium oleate in the presence of 50 ml of distilled water, 50 ml of ethanol, and 100 ml of hexane. Reaction was carried out at 70 °C for 4 h with a reflux condenser and then cooled to room temperature. The metal oleate solution was washed three times with 100 ml of distilled water using a separation funnel and then dried in a vacuum oven at 80 °C. To synthesize nanoparticles 25 g of metal oleate was mixed with 100 ml of 1-octadecene and 2 g of oleic acid at 100 rpm for 1 h using a vessel reactor with a reflux condenser. Temperature was raised to 320 °C using a heating rate of 3.5 °C/min. Afterward the reaction mixture was cooled to room temperature and the nanoparticles were washed with anhydrous ethanol (1:3 vol ratio), centrifuged at 7,798 g for 15 min, suspended in hexane (1:2.5 vol ratio), and centrifuged again at 555 g for 10 min. Any precipitated nanoparticles were removed by magnetic decantation, obtaining a stable colloid of magnetic nanoparticles coated with oleic acid and suspended in hexane.

Modification of the oleic acid-coated nanoparticles was carried out via ligand exchange with a functional amine-silane (APS). Acetic acid was used to promote hydrolysis of the trialkoxysilane structure in the APS molecule (Plueddemann 1982; De Palma et al. 2007). Hydrolysis of APS led to the formation of silanol (Si– OH) groups, which are condensed around the magnetic nanoparticle surface through siloxane (Si–O) bonds (Herrera et al. 2008; Coradin and Lopez 2003). In a typical functionalization, 6 mL of APS and 50 μL of acetic acid were added to 115 ml of the colloid formed by magnetic oleic acid nanoparticles suspended in hexane. This solution was mechanically stirred at room temperature for 3 days. During this process, nanoparticles coated with APS precipitate from the organic medium. Afterward, the precipitated APS-coated nanoparticles were removed by magnetic decantation and washed three times with 50 ml of hexane and once with 50 ml of ethanol. The functionalized magnetic nanoparticles were dried at room temperature.

Preparation of carboxymethyl-substituted dextrans (CMDx)

CMDx were prepared by a carboxymethylation reaction, where monochloro acetic acid reacted with dextran and sodium hydroxide (Chaubet et al. 1995; Huynh and Jozefonvicz 1998). Sodium hydroxide concentrations between 2 and 3 M were used to obtain different degrees of carboxymethylation. Dextran had a weight-average molecular weight M_w of 10 kDa and a polydispersity index of 1.1, as determined by gel permeation chromatography (GPC) using a Brookha-ven Instruments molecular weight analyzer BI-MwA and a PLaquagel-OH Mixed 8 μm column.

For a typical carboxymethylation reaction, 5 g of dextran were dissolved in 25 ml of distilled water and then cooled in an ice bath at approximately 4 °C. Subsequently, 17 ml of sodium hydroxide at concentrations of 2 or 3 M was added dropwise to the dextran solution. Then, 7.29 g of solid monochloroacetic acid were added. The reaction mixture was placed in a shaker with a water bath at 60 °C and stirred at 100 rpm for 75 min. Afterward the mixture was cooled to room temperature and then neutralized with glacial acetic acid. Finally, the product was precipitated and washed twice with ethanol, dialyzed to a conductivity ≤6 μS/cm, concentrated using a rotary evaporator, and dried at 60 °C.

After the carboxymethylation reaction, the modified dextrans are in the form of a carboxylate sodium salt ($-CH_2COONa$) (Huynh and Jozefonvicz 1998). An acid wash was used to obtain the free acid form ($-CH_2COOH$). For this, 1 g of CMDx was washed overnight with 14 ml of a solution of anhydrous methanol and nitric acid 70 %v/v (10:1). The acid liquor was removed by vacuum filtration and the solid product was subsequently washed several times with ethanol to remove all traces of the acid reagent and dried in a vacuum oven at 60 °C. Afterward, the amount of carboxylic (−COOH) groups per CMDx chain were determined by acidimetric titration (Eyler et al. 1947). For the acidimetric titration, we prepared solutions at 1 % w/v of CMDx in a mixture of distilled water/acetone

(1:1) with the addition of 10 ml of NaOH 0.012 N. This solution was titrated with hydrochloric acid 0.012 N, using phenolphthalein as indicator. From the titration data, the equivalents of −COOH groups per gram of CMDx were calculated using (Eyler et al. 1947)

$$A=\frac{V_{\mathrm{NaOH}}\times[C_{\mathrm{NaOH}}]-V_{\mathrm{HCl}}\times[C_{\mathrm{HCl}}]}{m} \quad (1)$$

where *A* is the milliequivalents of –COOH groups per gram of sample, *V* is the volume in L of NaOH or HCl used in the titration, *C* is the concentration of NaOH or HCl in mol/L, and *m* is the mass of CMDx expressed in grams.

The degree of substitution *DS* of the modified dextran is defined as the average number of sodium carboxymethyl groups per anhydroglucose unit. This value is calculated using (Huynh and Jozefonvicz 1998)

$$DS=\frac{162A}{100-80A} \quad (2)$$

where 162 is the molecular weight of an anhydroglucose unit and 80 is the molecular weight of the substituent group (–CH_2COONa). The degree of substitution *DS* is related to the number of –COOH groups N_{COOH} available per CMDx chain by

$$N_{\mathrm{COOH}}=\frac{M_{w-\mathrm{dex}}}{M_{w-\mathrm{unit}}}\times DS \quad (3)$$

where $M_{w\text{-dex}}$ is the molecular weight of the dextran and $M_{w\text{-unit}}$ is the molecular weight of the anhydroglucose unit.

According to the NaOH concentration used in the carboxymethylation reaction, we obtained two different carboxymethyl substituted dextrans, labeled CMDx-a and CMDx-b, for NaOH concentrations of 2 and 3 M, respectively. A third carboxymethyl substituted dextran, labeled CMDx-c, was obtained after a second carboxymethylation reaction performed using a sample of the carboxymethyl-substituted dextran prepared with NaOH 3 M. This second reaction step increases the incorporation of −COOH groups in the dextran chains (Chaubet et al. 1995).

Fluorescent carboxymethyl-substituted dextrans were prepared by conjugation of fluorescein-amine with CMDx molecules using carbodiimide chemistry. To obtain the fluorescent-CMDx molecules, we prepared a fluorescent solution using 50 mg of fluorescein-amine in 5 ml of ethanol in an amber vial. This fluorescent solution was cooled at 4 °C for 30 min and then it was reacted with 10 ml of an aqueous CMDx solution prepared at 0.013 M with the addition of 25 mg of EDC at pH 5.0 and previously cooled at 4 °C for 30 min. This reaction mixture was mechanically stirred at room temperature for 3 days. Afterward, free fluorescent molecules were removed by serial centrifugation in ethanol at 8,873 g for 30 min until a clear supernatant was obtained. The fluorescent-CMDx product was dried at 60 °C and stored in an amber vial at 8 °C.

Surface modification of magnetic-APS nanoparticles with CMDx

The carboxymethyl dextran was covalently bonded to the APS-coated nanoparticles using the carbodiimide molecule EDC (Herrera et al. 2008). In this surface modification, 0.1 g of APS-coated nanoparticles was suspended in 10 ml of deionized water at pH 5.0 using an

ultrasonic bath. This nanoparticle suspension was centrifuged at 3,500 rpm for 5 min to remove any precipitated nanoparticles. A CMDx solution was prepared by dissolving 2 g of CMDx in 10 ml of deionized water at pH 5.0. Afterward, 25 mg of EDC and 15 mg of NHS were added to the CMDx solution. The APS-coated nanoparticle suspension was mixed with the activated CMDx solution and then reacted at room temperature for 36 h at 150 rpm. Afterward, the functionalized nanoparticles were washed three times with ethanol (1:3 vol ratio) at 8,873 g for 20 min. Fluorescent nanoparticles were also prepared to visualize the interaction with cell membranes using confocal laser scanning microscopy (CLSM). For this purpose, we functionalized the synthesized APS-coated nanoparticles with fluorescent-CMDx.

Characterization of functionalized nanoparticles

Surface modification of the nanoparticles was confirmed by infrared spectroscopy using a Varian 800 FTIR and ZnSe ATR holder with a wavenumber ranging from 600 to 4,000 cm^{-1}. The size and size distribution of the nanoparticles were determined at different functionalization steps using a JEOL 1200EX transmission electron microscope (TEM). Hydrodynamic diameter and zeta potential were measured using a Brookhaven Instruments BI-90 Plus particle size and zeta potential analyzer. A Quantum Design MPMS XL-7 SQUID magnetometer was used to determine the magnetic properties of the nanoparticles. Cell viability was analyzed with a Molecular Devices SpectraMax Gemini EM spectrofluorometer. An Olympus Fluoview FV 300 IX71 confocal laser scanning microscope (CLSM) was used to visualize the nanoparticle's interaction with the cancer cells.

CaCo-2 Cell culture

Cells were cultured in 75 cm^2 cell culture flasks using Dulbecco's Modified Eagle Medium (DMEM) containing 10 % fetal bovine serum (FBS), 1 % nonessential amino acids, 10 mL of penicillin, 100 ug/mL of streptomycin, 0.876 g/L of L-glutamine, and 2.7 g/L of sodium bicarbonate. Cells were maintained in a controlled atmosphere at 37 °C, 95 % relative humidity, and 5 % CO_2. The culture medium was changed every third day for a week until cells reached ~80-90 % confluency. Cells were detached from the culture flask by trypsinization and resuspended in culture medium.

Visualization of nanoparticle internalization in CaCo-2 cells

For visualization of fluorescent-CMDx-coated magnetic nanoparticles with different surface charges in contact with CaCo-2 cancer cells, 50,000 cells were seeded in chambered coverslips (Lab-Tek®, Cat. Number 155380) in DMEM+10 % FBS and allowed to grow overnight. Each type of fluorescent nanoparticle was suspended in DMEM+10 % of FBS at a concentration of 1.0 mg of iron oxide/mL. This nanoparticle suspension was placed in contact with the cells for 24 h. Afterward, the nanoparticle suspension was removed by aspiration. Samples were washed twice with fresh DMEM+10 % FBS to remove any particles not attached to the cell membrane. The cell membrane was stained with a solution of 5 μL Vybrant DiD (Molecular Probes®, Invitrogen, CA) in 1 mL DMEM+10 % FBS for 20 min at 37 °C, and washed twice with media to remove excess of fluorescent dye. The cell nucleus was stained for 5 min at 37 °C using a 13 nM DAPI (Molecular Probes, Invitrogen, CA) solution in PBS, cells were rinsed twice with PBS to remove excess nuclear stain. Nanoparticle internalization in cells was visualized by Confocal Laser Scanning Microscopy (FV300, Olympus America, NY).

Quantification of cellular uptake of nanoparticles in CaCo-2 cells

CaCo-2 cells (500,000) were seeded in sterile 6-well plates (3502, Falcon, Corning, NY) and allowed to reach confluence. A solution consisting of DMEM+10 % FBS and 1 mg iron oxide/mL of each type of nanoparticle were put in contact with cells for 24 h at 37 °C. After incubation, the nanoparticle solution was removed, cells were washed twice with DMEM +10 % FBS, washed once with EDTA, and were then trypsinized and counted manually with a hemacytometer. Cells were pelleted by centrifugation and supernatant was removed. Cell pellets were digested with 200 μL 70 % nitric acid at 100 °C for 1 h to convert iron oxide into free iron and diluted to 4 mL with milli-Q water. Iron content was measured by Inductively Coupled Plasma Mass Spectroscopy (ICP-MS) using an Agilent 7500ce. Internalized iron is reported as pg iron/cell.

In order to determine the surface charge dependence of the nanoparticle internalization mechanism in CaCo-2 cells, samples were processed as follows: 500,000 CaCo-2 cells were seeded in sterile 6-well plates (3502, Falcon, Corning, NY) and allowed to reach confluence. A solution consisting of a known endocytosis inhibitor in media (DMEM+10 % FBS) was added to cells and incubated for 1 h. After this preincubation, media were removed and a solution consisting of each endocytosis inhibitor and 1 mg iron oxide/mL of each type of nanoparticle with a different surface charge in DMEM+10 % FBS was put in contact with cells for 24 h at 37 °C. Fluid-phase endocytosis (FPE) was inhibited by adding 100 μM 5-(*N*-ethyl-*N*-isopropyl) amiloride to nanoparticle solution, a concentration that has been demonstrated to inhibit the internalization of dextran in CaCo-2 cells (Ivanov et al. 2004). Dansylcadaverine inhibits the internalization of transferrin, a protein which is internalized through clathrin-mediated endocytosis (McMahon and Boucrot 2011). This pathway was blocked by the addition of 500 μM dansyl-cadaverine to nanoparticle solution, a concentration which effectively inhibits the entry of transferrin into various cell lines cells (Schapiro et al. 1998; Orlandi and Fishman 1998). Filipin is a pharmacological agent routinely used to block the internalization of the cholera toxin subunit-β. 1 μg/mL of fillipin in nanoparticle solution was used to inhibit the caveola-mediated mechanism of internalization into CaCo-2 cells, an amount which has been shown to obstruct the entry of the cholera toxin subunit-β (Navarro-García et al. 2007). Cell pellets with internalized nanoparticles were washed, trypsinized, counted, digested, and diluted as described above. Iron was measured by ICP-MS and reported as pg Fe/cell.

Results and discussion

Chemical structure of the carboxymethyl-substituted dextrans and modification of nanoparticle surface

The bonding of −COOH groups in the CMDx was confirmed by infrared spectroscopy. For these measurements, CMDx in powder form was used without further preparation. Figure 1 illustrates these measurements from which we can observe in the IR spectra (a) the characteristic peaks of the dextran molecule, which has bands at 2900, 1040, and 917 cm^{-1}, attributed to the presence of C−H bonds, C−O bonds, and the α-glucopyranose ring, respectively (Jung 1995; Lin-Vien et al. 1991). After carboxymethylation reaction and acid wash, we observed for CMDx-a, CMDx-b, and CMDx-c the presence of a band at 1,730 cm^{-1}, as indicated in curves (b), (c), and (d), respectively. This band is characteristic of the carboxylic acid group in the free acid form (–COOH). The intensity of this band can be qualitatively related to the amountof–COOH groupsincorporatedinthe modified dextran chains, as we observe small signal intensity for CMDx-a and strong signal intensities for CMDx-b, and CMDx-c. According to acidimetric titration the number of –COOH groups per chain are ∼5, 23, and 38 for the a, b, and c samples, as summarized in Table 1.

Coating of the nanoparticles with APS and CMDx was also confirmed by infrared spectroscopy (see Supporting Information Figure S1). For these measurements, dry and pulverized particles were used without further manipulation. We observed characteristic vibrational bands at 2,920 and 2,850 cm^{-1} for the as-synthesized magnetic nanoparticles, which were attributed to the antisymmetric and symmetric $–CH_2$ stretching present in the structure of the oleic acid (Lin-Vien et al. 1991). Furthermore, we observed a band at 1,720 cm^{-1} which was attributed to the antisymmetric C=O stretch of the carboxylic acid (De Palma et al. 2007). After ligand exchange, we observed for nanoparticles coated with APS bands at about 1,630 and 1,550 cm^{-1} characteristic of the $– NH_2$ bending mode of free amino groups and C–N stretching mode present in the APS structure (Yamaura et al. 2004; Lin-Vien et al. 1991). Furthermore, we observed the presence of bands at about 1100, 1000, and 920 cm^{-1}, which correspond to the condensation of siloxane (Si–O) molecules onto the surface of the magnetic nanoparticles (Mornet et al. 2004; Yamaura et al. 2004). The presence of these bands and the absence of the bands attributed to the oleic acid indicate successful ligand exchange (De Palma et al. 2007). Grafting of CMDx molecules onto the modified magnetic APS nanoparticles was confirmed by the existence of bands at about 3250, 1590, and 1150 cm^{-1} in the spectrum of magnetic APS-CMDx nanoparticles. These bands correspond to the N–H stretch mode, the –C(=O)–N–H secondary amine bond, and the antisymmetric stretch of the C–N–C secondary amine moiety, respectively (Lin-Vien et al. 1991). We attribute the formation of the secondary amine bond to the link between amine groups previously grafted onto the nanoparticles surface and the carboxyl groups present in the CMDx chains.

Nanoparticle size and morphology

The physical size and size distribution of the magnetic nanoparticles was observed by TEM measurements at various stages of the preparation process. The ImageJ program was used to measure the diameters of one hundred nanoparticles, which were fitted to a lognormal size distribution (see Supporting Information, Figure S2 for histograms of particle size distribution). Samples of magnetic nanoparticles coated with oleic acid suspended in hexane, magnetic APS nanoparticles suspended in deionized water at pH 5.0, and magnetic APS-CMDx nanoparticles suspended in deionized water were prepared. Subsequently, ultrathin carbon type A grids were immersed in these nanoparticle solutions, placed on filter paper, and then dried in a vacuum oven for 30 min.

Figure 2a shows a representative image of the magnetic nanoparticles synthesized using the thermal decomposition method, displaying the formation of separate nanoparticles with size of 13 ± 1 nm for the oleic acid-coated nanoparticles. No significant nanoparticle agglomeration was observed after the ligand exchange of oleic acid with the APS molecules, Fig. 2b, or after grafting of CMDx molecules onto the nanoparticles surface, Fig. 2c, resulting in nanoparticles with sizes of 13 ± 1 nm for the APS-coated nanoparticles and 13 ± 2 nm for the CMDx-coated nanoparticles.

Determination of the hydrodynamic diameter of the functionalized nanoparticles

Dynamic light scattering (DLS) was used to measure the hydrodynamic diameter of the magnetic nanoparticles at the different functionalization steps (see Supporting Information, Figure S3 for hydrodynamic diameter distributions). For these measurements, we prepared colloidal dispersions of oleic acid-coated nanoparticles in hexane, APS-coated nanoparticles in deionized water at pH 5.0, and APS-CMDx-coated nanoparticles in deionized water. Colloidal dispersions prepared in hexane were filtered with 0.1 μm PTFE filter syringes, while those prepared in deionized water were filtered with 0.2-μm nylon filter syringes. We observed a hydrodynamic diameter of 19 ± 1 nm for the oleic acid-coated nanoparticles and 20 ± 1 nm for the APS-coated nanoparticles. The similarity in hydrodynamic diameter

between these two steps indicates that a thin coating of APS was deposited on the nanoparticles. For the CMDx-coated nanoparticles the hydrodynamic diameters were 33 ± 2 nm for IO-CMDx-a,39 ± 3 nmfor IO-CMDx-b, and45 ± 7 nm for IO-CMDx-c. An increase in hydrodynamic diameter was tobe expected upon coating with CMDx, and a slight increase in hydrodynamic diameter with increasing degree of substitution in the CMDx can perhaps be explained by electrostatic repulsion extending the CMDx into the surrounding medium.

The hydrodynamic diameter of nanoparticles coated with CMDx-a, CMDx-b, and CMDx-c was measured as a function of pH and ionic strength. For these measurements we suspended the CMDx-coated nanoparticles in 30 ml of deionized water at 0.5 % w/v with the addition of 0.3 ml of KNO_3 1.0 mM. Figure 3 shows that the hydrodynamic diameter of the func-tionalized nanoparticles did not change significantly with variations in pH from 2 to 10. Additionally, Fig. 4 shows that the hydrodynamic diameter of the func-tionalized nanoparticles did not change significantly with increasing concentration of NaCl, up to 0.14 M.

Zeta potential measurements

The surface charge and isoelectric point of magnetic nanoparticles coated with the CMDX were studied by zeta potential measurements. For these measurements the CMDx-coated magnetic nanoparticles were suspended at 0.5 % w/v in 1 mM KNO_3. The pH of the solution was then varied from 2 to 12.0 by titration with KOH and HNO_3. Results are presented in Fig. 5. The isoelectric point of APS-coated nanoparticles was observed at pH 10.0, as in other studies (De Palma et al. 2007; Mornet et al. 2005; Herrera et al. 2008). In the case of CMDx-coated magnetic nanoparticles, the isoelectric point was observed near pH 2 for all samples. This is attributed to –COOH groups remaining in the bonded CMDx chains, which impart a negative charge over almost the entire pH range. It is important to mention that the particles were stable in the whole pH range and no precipitation was observed. This observation suggests that nanoparticle stabilization occurred by steric repulsion. Also, we note that by decreasing the carboxylic group content the nanoparticle surface charge significantly decreases without affecting stability.

The zeta potential of the CMDx-coated magnetic nanoparticles was also measured at varying NaCl concentrations to study the effect of ionic strength on surface charge and stability. For these measurements the modified nanoparticles were suspended in deionized water at pH 7.0, as described previously. Figure 6 shows a decrease in zeta potential of the CMDx-coated magnetic nanoparticles with increasing concentration of NaCl, up to 0.14 M. This decrease was dependent on the number of –COOH groups incorporated in the dextran chains. In the case of nanoparticles coated with CMDx-c (38 –COOH/chain, as determined by acidimetric titration) we observed a surface charge decrease from −50 to −20 mV. For nanoparticles modified with CMDx-b molecules (23 –COOH/chain) we observed a surface charge decrease from −25 to −15 mV. In the case of magnetic nanoparticles functionalized with CMDx-a (5 –COOH/chain) the surface charge shifted from −20 mV to +5 mV.

Visualization of fluorescent magnetic nanoparticles uptake in CaCo-2 cells

Fluorescent nanoparticles in contact with cells were visualized by confocal laser scanning microscopy using an Olympus Fluoview FV 300 IX71 (Fig. 7). Nuclear cell staining was observed through a DAPI filter, DiD membrane staining was observed through a Cy5 filter, and fluorescent magnetite-APS-CMDx-c nanoparticles were visualized with a fluorescein isothiocyanate (FITC) filter. In Fig. 7 the stained nucleus is visualized as blue, the fluorescent nanoparticles as green, and the cell membrane as red. We observed surface charge-specific differences in CMDx-coated nanoparticle internalization, as shown in Fig. 7.

The more negatively charged nanoparticles accumulated in larger vesicles more significantly than the less negatively charged nanoparticles.

Surface charge-dependent nanoparticle uptake in CaCo-2 cells

Iron oxide nanoparticles coated with carboxymethyl dextran with varying degrees of –COOH substitution were incubated with CaCo-2 cells and internalized iron oxide was measured by ICP-MS. As seen in Fig. 8, there was a clear correlation between increasing negative surface charge and nanoparticle internalization. This is most likely due to differences in nanoparticle surface charge and cell membrane interactions.

We assessed the role of surface charge in nanoparticle cellular internalization by inhibiting known mechanisms of internalization with known endocytosis inhibitors. Amiloride was used to inhibit fluid-phase endocytosis, a mechanism by which molecules and fluids surrounding the cell are internalized non-specifically (Posner et al. 1982). Treatment with Amiloride inhibited the uptake of IO-CMDx-a and IO-CMDx-b. Particles with a more negative surface charge (IO-CMDx-c) seemed to be inhibited, but not as significantly. This suggests that CMDx-coated nanoparticles with highly negative surface charge can enter the cell through non-specific nanoparticle/cell interactions. Dansylcadaverine and fillipin were used to inhibit two different receptor-mediated cell internalization pathways; clathrin-mediated and caveolae-mediated endocytosis. Both internalization pathways depend on specific protein–receptor interactions. The most significant difference between these pathways is their intracellular fate. Molecules internalized via the clathrin pathway end up trapped in the endo/lysosomal pathway, while molecules internalized via the caveolae-dependent pathway can escape into the endoplasmic reticulum. Dansylcadaverine and fillipin seem to exert their most inhibitory effect on the internalization of nanoparticles with the most negative surface charge (CMDx-c). Since there are no known receptors for carboxymethyl dextran, this effect could be due to the formation of a protein corona around nanoparticles, formed through non-specific interactions between nanoparticles and serum proteins that are normally internalized through clathrin- and caveolae-dependent pathways. A recent study by Rauch and colleagues shows that dextran−COOH-coated SPIONS are in fact able to interact with EGF protein receptors, which are internalized through a clathrin-mediated pathway (Rauch et al. 2012). The authors propose that this phenomenon is possibly activated through the adsorption of ligands found in cell culture media onto the nanoparticle surface, and the binding of these ligands onto receptors.

Conclusions

The effect of surface charge on uptake of iron oxide nanoparticles by CaCo-2 cells was evaluated. Monodisperse, colloidally stable iron oxide nanoparticles coated with carboxymethyl dextran with varying degrees of substitution of carboxylic groups (–COOH) were prepared. Results showed that increasing the number of carboxylic groups per dextran chain increased the nanoparticle's surface charge without affecting their colloidal stability at physiological conditions. We observed an increase in the amount of iron oxide internalized by CaCo-2 cells when incubated with the most negatively charged iron oxide nanoparticles, confirming that particle–cell interactions are charge-dependent. Internalization of iron oxide nanoparticles coated with CMDx-a and CMDx-b was significantly inhibited when fluid-phase endocytosis inhibitors were used. This suggests that the uptake of these nanoparticles by CaCo-2 cells occurs mainly via non-specific interactions. Uptake of CMDx-c-coated iron oxide nanoparticles was reduced when two different receptor-mediated pathways were inhibited. This effect was attributed to non-specific interaction between CMDx-c-coated iron oxide nanoparticles and serum proteins internalized by those receptors in CaCo-2 cells. Overall, we see a correlation between particle surface charge and particle–cell interactions. Thus, future work would take into consideration various “cell observers” to investigate the

role of cell type. Finally, we suggest the particles obtained in this work as an ideal system to further study the impact of surface charge in the nanoparticle–cell interactions.

Supplementary Material

Refer to Web version on PubMed Central for supplementary material.

Acknowledgments

This work was supported by the US NSF (CBET-0609117, OIA-0701525) and tNIH (1 R15 EB010228-01). We acknowledge the use of the Integrated Advanced Microscopy facility at the Cornell Center for Materials Research (CCMR) supported by the NSF-MRSEC program (DMR 0520404) and are grateful to Prof. Juan Hinestroza and Alejandra Andere for performing TEM measurements. We acknowledge the use of the UPRM microscopy facility and the help of Mr. Jose Almodóvar in the CLSM measurements.

References

Alhareth K, Vauthier C, Bourasset F, Gueutin C, Ponchel G, Moussa F. Conformation of surface-decorating dextran chains affects the pharmacokinetics and biodistribution of doxorubicin-loaded nanoparticles. Eur J Pharm Biopharm. 2012; 81(2):453–457. [PubMed: 22465096]

Arias JL, Lopez-Viota M, Saez-Fernandez E, Ruiz MA, Delgado AV. Engineering of an antitumor (core/shell) magnetic nanoformulation based on the chemotherapy agent ftorafur. Colloids Surf A. 2011; 384(1–3):157–163t.

Arnida, Janát-Amsbury MM, Ray A, Peterson CM, Ghandehari H. Geometry and surface characteristics of gold nanoparticles influence their biodistribution and uptake by macrophages. Eur J Pharm Biopharm. 2011; 77(3):417–423. 10.1016/j.ejpb.2010.11.010. [PubMed: 21093587]

Bahmani B, Gupta S, Upadhyayula S, Vullev VI, Anvari B. Effect of polyethylene glycol coatings on uptake of indocyanine green loaded nanocapsules by human spleen macrophages in vitro. J Biomed Opt. 2011; 16 10.1117/1.3574761.

Bao N, Shen L, Wang Y, Padhan P, Gupta A. A facile thermolysis route to monodisperse ferrite nanocrystals. J Am Chem Soc. 2007; 129:12374–12375. [PubMed: 17880220]

Bhattacharya D, Sahu SK, Banerjee I, Das M, Mishra D, Maiti TK, Pramanik P. Synthesis, characterization, and in vitro biological evaluation of highly stable diversely functionalized superparamagnetic iron oxide nanoparticles. J Nanopart Res. 2011; 13(9):4173–4188. 10.1007/s11051-011-0362-7.

Chao Y, Karmali PP, Simberg D. Role of carbohydrate receptors in the macrophage uptake of dextran-coated iron oxide nanoparticles. Adv Exp Med Biol. 2012; 733:115–123. [PubMed: 22101717]

Chaubet J, Maiga O, Mauray S, Jozefonvicz J. Synthesis and structure-anticoagulant property relationships of functionalized dextrans. Carbohydr Polym. 1995; 28:145–152.

Chen JP, Yang PC, Ma YH, Lu YJ. Superparamagnetic iron oxide nanoparticles for delivery of tissue plasminogen activator. J Nanosci Nanotechnol. 2011; 11(12):11089–11094. [PubMed: 22409062]

Cole AJ, David AE, Wang J, Galbán CJ, Hill HL, Yang VC. Polyethylene glycol modified, cross-linked starchcoated iron oxide nanoparticles for enhanced magnetic tumor targeting. Biomaterials. 2011; 32(8):2183–2193. 10. 1016/j.biomaterials.2010.11.040. [PubMed: 21176955]

Cooper, GM.; Hausman, RE. The cell: a molecular approach. 5th. Sinauer Associates; Sunderland: 2009. Lysosomes.

Coradin T, Lopez P. Biogenic silica patterning: simple chemistry or subtle biology? ChemBioChem. 2003; 3:1–9.

Creixell M, Herrera AP, Latorre-Esteves M, Ayala V, Torres-Lugo M, Rinaldi C. The effect of grafting method on the colloidal stability and in vitro cytotoxicity of carboxymethyl dextran coated magnetic nanoparticles. J Mater Chem. 2010; 20(39):8539–8547. 10.1039/c0jm01504k.

Creixell M, Bohorquez AC, Torres-Lugo M, Rinaldi C. EGFR-targeted magnetic nanoparticle heaters kill cancer cells without a perceptible temperature rise. ACS Nano. 2011; 5(9):7124–7129. 10.1021/nn201822b. [PubMed: 21838221]

de Chickera SN, Snir J, Willert C, Rohani R, Foley R, Foster PJ, Dekaban GA. Labelling dendritic cells with SPIO has implications for their subsequent in vivo migration as assessed with cellular MRI. Contrast Media Mol Imaging. 2011; 6(4):314–327. 10.1002/cmmi.433. [PubMed: 21861291]

De Palma R, Peeters S, Van Bael M, Van den Rul H, Bonroy K, Laureyn W, Mullens J, Borghs G, Maes G. Silane ligand exchange to make hydrophobic superparamagnetic nanoparticles water-dispersible. Chem Mater. 2007; 19:1821–1831.

Dubiel EA, Kuehn C, Wang R. Vermette P In vitro morphogenesis of PANC-1 cells into islet-like aggregates using RGD-covered dextran derivative surfaces. Colloids Surf B Biointerfaces. 2012; 89(0):117–125. 10.1016/j.colsurfb.2011.09.003. [PubMed: 21962947]

Eyler RW, Klug ED, Diephuis F. Determination of degree of substitution of sodium carboxymethylcellulose. Anal Chem. 1947; 19(1):24–27.

French RA, Jacobson AR, Kim B, Isley SL, Penn RL, Baveye PC. Influence of ionic strength, pH, and cation valence on aggregation kinetics of titanium dioxide nanoparticles. Environ Sci Technol. 2009; 43(5):1354–1359. 10.1021/es802628n. [PubMed: 19350903]

Gautier J, Munnier E, Paillard A, Herve K, Douziech-Eyrolles L, Souce M, Dubois P, Chourpa I. A pharmaceutical study of doxorubicin-loaded PEGylated nanoparticles for magnetic drug targeting. Int J Pharm. 2012; 423(1):16–25. [PubMed: 21703340]

Ge Y, Zhang Y, Xia J, Ma M, He S, Nie F, Gu N. Effect of surface charge and agglomerate degree of magnetic iron oxide nanoparticles on KB cellular uptake in vitro. Colloids Surf B. 2009; 73(2): 294–301. 10.1016/j.colsurfb.2009.05.031.

Georgieva JV, Kalicharan D, Couraud PO, Romero IA, Weksler B, Hoekstra D, Zuhorn IS. Surface characteristics of nanoparticles determine their intracellular fate in and processing by human blood-brain barrier endothelial cells in vitro. Mol Ther. 2011; 19(2):318–325. 10.1038/mt.2010.236. [PubMed: 21045812]

Gratton SEA, Ropp PA, Pohlhaus PD, Luft JC, Madden VJ, Napier ME, DeSimone JM. The effect of particle design on cellular internalization pathways. Proc Natl Acad Sci USA. 2008; 105(33): 11613–11618. 10.1073/pnas.0801763105. [PubMed: 18697944]

Grenha A. Chitosan nanoparticles: a survey of preparation methods. J Drug Target. 2012; 20(4):291–300. 10.3109/1061186X.2011.654121. [PubMed: 22296336]

Guarnieri D, Guaccio A, Fusco S, Netti P. Effect of serum proteins on polystyrene nanoparticle uptake and intracellular trafficking in endothelial cells. J Nanopart Res. 2011; 13(9):4295–4309. 10.1007/s11051-011-0375-2.

Häfeli UO, Riffle JS, Harris-Shekhawat L, Carmichael-Baranauskas A, Mark F, Dailey JP, Bardenstein D. Cell uptake and in vitro toxicity of magnetic nanoparticles suitable for drug delivery. Mol Pharm. 2009; 6(5):1417–1428. 10.1021/mp900083m. [PubMed: 19445482]

Han GC, Ouyang Y, Long XY, Zhou Y, Li M, Liu YN, Kraatz HB. (Carboxymethyl-Dextran)-modified magnetic nanoparticles conjugated to octreotide for MRI applications. Eur J Inorg Chem. 2010; 34:5455–5461. 10.1002/ejic.201000715.

Herrera AP, Barrera C, Rinaldi C. Synthesis and func-tionalization of magnetite nanoparticles with aminopropylsilane and carboxymethyl-dextran. J Mater Chem. 2008; 18:3650–3654. 10.1039/B805256E.

Huang J, Zhao R, Wang H, Zhao W, Ding L. Immobilization of glucose oxidase on Fe3O4/SiO2; magnetic nanoparticles. Biotechnol Lett. 2010; 32(6):817–821. 10.1007/s10529-010-0217-9. [PubMed: 20155486]

Huynh F, Jozefonvicz J. Carboxymethylation of dextran in aqueous alcohol as the first step of the preparation of derivatized dextrans. Die Angew Makromol Chem. 1998; 254:61–65.

Ivanov AI, Nusrat A, Parkos CA. Endocytosis of epithelial apical junctional proteins by a clathrin-mediated pathway into a unique storage compartment. Mol Biol Cell. 2004; 15(1):176–188. 10.1091/mbc.E03-05-0319. [PubMed: 14528017]

Jedlovszky-Hajdú A, Bombelli FB, Monopoli MP, Tombácz E, Dawson KA. Surface coatings shape the protein corona of SPIONs with relevance to their application in vivo. Langmuir. 2012; 28(42): 14983–14991. 10.1021/la302446h. [PubMed: 23002920]

Jung C. Surface properties of superparamagnetic iron oxide MR contrast agents: ferumoxides, ferumoxtran, ferumoxsil. Magn Reson Imaging. 1995; 13:675–691. [PubMed: 8569442]

Jung, BS.; Lomeli, E.; Anvari, B. Effect of coating material on uptake of indocyanine green-loaded nanocapsules by HeLa cervical cancer cells. In: Jansen, ED.; Thomas, RJ., editors. Optical interactions with tissues and cells XXI. Vol. 7562. Proc SPIE; 2010. 10.1117/12.842754

Jung MJ, Ha YE, Lee DY. Heparin-coated superparamagnetic iron oxide nanoparticles as highly effective MRI contrast agent for cell labeling. J Control Release. 2011; 152(Suppl 1):e214–e215. [PubMed: 22195863]

Klostergaard J, Seeney CE. Magnetic nanovectors for drug delivery. Maturitas. 2012; 73(1):33–44. [PubMed: 22402027]

Laurent S, Dutz S, Haefeli UO, Mahmoudi M. Magnetic fluid hyperthermia: focus on superparamagnetic iron oxide nanoparticles. Adv Colloid Interface Sci. 2011; 166(1–2):8–23. 10.1016/j.cis.2011.04.003. [PubMed: 21601820]

Laurent S, Burtea C, Thirifays C, Häfeli UO, Mahmoudi M. Crucial ignored parameters on nanotoxicology: the importance of toxicity assay modifications and “cell vision”. PLoS One. 2012; 7(1):e29997. 10.1371/journal.pone.0029997. [PubMed: 22253854]

Laurent S, Burtea C, Thirifays C, Rezaee F, Mahmoudi M. Significance of cell “observer” and protein source in nanobiosciences. J Colloid Interface Sci. 2013; 392(0):431–445. org/10.1016/j.jcis.2012.10.005. [PubMed: 23141702]

Li D, Teoh WY, Gooding JJ, Selomulya C, Amal R. Functionalization strategies for protease immobilization on magnetic nanoparticles. Adv Funct Mater. 2010; 20(11):1767–1777. 10.1002/adfm.201000188.

Lin-Vien, D.; Colthup, N.; Fateley, W.; Graselli, J. The handbook of infrared and Raman characteristic frequencies of organic molecules. Academic Press; San Diego: 1991.

Mahmoudi M, Saeedi-Eslami SN, Shokrgozar MA, Azadmanesh K, Hassanlou M, Kalhor HR, Burtea C, Rothen-Rutishauser B, Laurent S, Sheibani S, Vali H. Cell “vision”: complementary factor of protein corona in nanotoxicology. Nanoscale. 2012; 4(17):5461–5468. [PubMed: 22842341]

Manju S, Sreenivasan K. Enhanced drug loading on magnetic nanoparticles by layer-by-layer assembly using drug conjugates: blood compatibility evaluation and targeted drug delivery in cancer cells. Langmuir. 2011; 27(23):14489–14496. 10.1021/la202470k. [PubMed: 21988497]

McMahon HT, Boucrot E. Molecular mechanism and physiological functions of clathrin-mediated endocytosis. Nat Rev Mol Cell Biol. 2011; 12(8):517–533. 10.1038/nrm3151. [PubMed: 21779028]

Mikhaylov G, Vasiljeva O. Promising approaches in using magnetic nanoparticles in oncology. Biol Chem. 2011; 392:955–960. 10.1515/bc.2011.185. [PubMed: 21848508]

Miles WC, Goff JD, Huffstetler PP, Reinholz CM, Pothayee N, Caba BL, Boyd JS, Davis RM, Riffle JS. Synthesis and colloidal properties of polyetherâ^'magnetite complexes in water and phosphate-buffered saline. Langmuir. 2008; 25(2):803–813. 10.1021/la8030655. [PubMed: 19105718]

Modi S, Swetha MG, Goswami D, Gupta GD, Mayor S, Krishnan Y. A DNA nanomachine that maps spatial and temporal pH changes inside living cells. Nat Nano. 2009; 4(5):325–330. 10.1038/nnano.2009.83.

Mornet S, Vasseur S, Grasset F, Duguet E. Magnetic nanoparticle design for medical diagnosis and therapy. J Mater Chem. 2004; 14:2161–2175.

Mornet S, Portier J, Duguet E. A method for synthesis and functionalization of ultrasmall supeparamagentic covalent carriers based on maghemite and dextran. J Magn Magn Mater. 2005; 293:127–134.

Navarro-García F, Canizalez-Roman A, Vidal JE, Salazar MI. Intoxication of epithelial cells by plasmid-encoded toxin requires clathrin-mediated endocytosis. Microbiology. 2007; 153(9):2828–2838. 10.1099/mic.0.2007/007088-0. [PubMed: 17768228]

Ning S, Huang Q, Sun X, Li C, Zhang Y, Li J, Liu YN. Carboxymethyl dextran-coated liposomes: toward a robust drug delivery platform. Soft Matter. 2011; 7(19):9394–9401.

Orlandi PA, Fishman PH. Filipin-dependent inhibition of cholera toxin: evidence for toxin internalization and activation through caveolae-like domains. J Cell Biol. 1998; 141(4):905–915. 10.1083/jcb.141.4.905. [PubMed: 9585410]

Osakaa T, Nakanishib T, Shanmugama S, Takahamaa S, Zhangb H. Effect of surface charge of magnetite nanoparticles on their internalization into breast cancer and umbilical vein endothelial cells. Colloids Surf B. 2009; 71:325–330.

Park K, Hwang Y, Park J, Noh H, Kim J, Hwang N, Hyeon T. Ultra large-scale synthesis of monodisperse nanocrystals. Nat Mater. 2004; 3:891–895. [PubMed: 15568032]

Phadatare MR, Khot VM, Salunkhe AB, Thorat ND, Pawar SH. Studies on polyethylene glycol coating on NiFe(2)O(4) nanoparticles for biomedical applications. J Magn Magn Mater. 2012; 324(5):770–772. 10.1016/j.jmmm.2011.09.020.

Plueddemann, E. Silane coupling agents. Plenum Press; New York: 1982.

Posner BI, Khan MN, Bergeron JJ. Endocytosis of peptide hormones and other ligands. Endocr Rev. 1982; 3(3):280–298. 10.1210/edrv-3-3-280. [PubMed: 6126355]

Pradhan P, Giri J, Banerjee R, Bellare J, Bahadur D. Cellular interactions of lauric acid and dextran-coated magnetite nanoparticles. J Magn Magn Mater. 2007; 311:282–287.

Rauch J, Kolch W, Mahmoudi M. Cell type-specific activation of AKT and ERK signaling pathways by small negatively-charged magnetic nanoparticles. Sci Rep. 2012; 2:868. [PubMed: 23162692]

Ravikumar C, Kumar S, Bandyopadhyaya R. Aggregation of dextran coated magnetic nanoparticles in aqueous medium: experiments and Monte Carlo simulation. Colloids Surf A. 2012; 403:1–6.

Santosh S, Podaralla P, Miller B. Anaphylaxis with elevated serum tryptase after administration of intravenous ferumoxytol. NDT Plus. 2010; 3(4):341–342. 10.1093/ndtplus/sfq084.

Schapiro FB, Lingwood C, Furuya W, Grinstein S. pH-independent retrograde targeting of glycolipids to the Golgi complex. A J Physiol Cell Physiol. 1998; 274(2):C319–C332.

Thorek DLJ, Tsourkas A. Size, charge and concentration dependent uptake of iron oxide particles by non-phagocytic cells. Biomaterials. 2008; 29(26):3583–3590. [PubMed: 18533252]

Veiseh O, Gunn JW, Zhang M. Design and fabrication of magnetic nanoparticles for targeted drug delivery and imaging. Adv Drug Deliv Rev. 2010; 62(3):284–304. 10. 1016/j.addr.2009.11.002. [PubMed: 19909778]

Villanueva A, Magdalena C, Alejandro GR, Macarena C, Sa-bino VV, Carlos JS, María del Puerto M, Rodolfo M. The influence of surface functionalization on the enhanced internalization of magnetic nanoparticles in cancer cells. Nanotechnology. 2009; 20(11):115103. [PubMed: 19420433]

Walczyk D, Bombelli FB, Monopoli MP, Lynch I, Dawson KA. What the cell “sees” in bionanoscience. J Am Chem Soc. 2010; 132(16):5761–5768. 10.1021/ja910675v. [PubMed: 20356039]

Wilhelm C, Billotey C, Roger J, Pons JN, Bacri JC, Gazeau F. Intracellular uptake of anionic superparamagnetic nanoparticles as a function of their surface coating. Biomaterials. 2003; 24(6): 1001–1011. 10.1016/s0142-9612(02)00440-4. [PubMed: 12504522]

Wotschadlo J, Liebert T, Heinze T, Wagner K, Schnabelrauch M, Dutz S, Mueller R, Steiniger F, Schwalbe M, Kroll TC, Hoeffken K, Buske N, Clement JH. Magnetic nanoparticles coated with carboxymethylated polysaccharide shells-Interaction with human cells. J Magn Magn Mater. 2009; 321(10):1469–1473. 10.1016/j.jmmm.2009.02. 069.

Xu H, Aguilar ZP, Yang L, Kuang M, Duan H, Xiong Y, Wtiei H, Wang A. Antibody conjugated magnetic iron oxide nanoparticles for cancer cell separation in fresh whole blood. Biomaterials. 2011; 32(36):9758–9765. [PubMed: 21920599]

Yamaura M, Camilo RL, Sampaio LC, Macedo MA, Nakamura M, Toma HE. Preparation and characterization of (3-aminopropyl) triethoxysilane-coated magnetite nanoparticles. J Magn Magn Mater. 2004; 279:210–217.

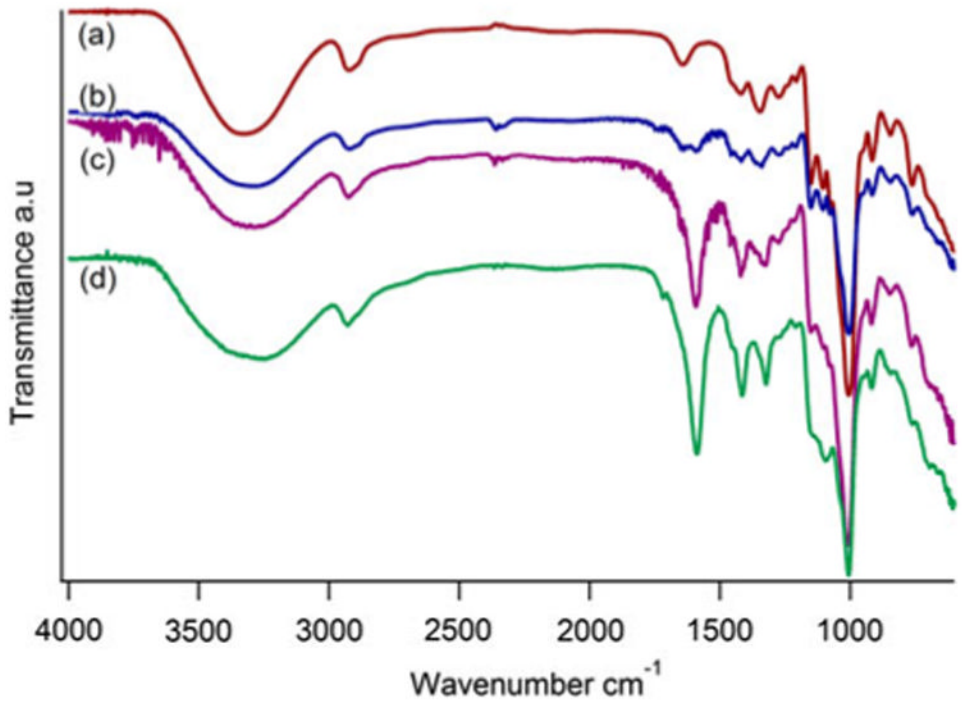

Fig. 1.

FTIR spectra of carboxymethyl-substituted dextrans as obtained after the carboxymethylation reaction and acid wash. Curve (*a*) represents non-modified dextran. Curve (*b*) illustrates the substituted dextran CMDx-a, curve (*c*) is for CMDx-b, and curve (*d*) is for CMDx-c

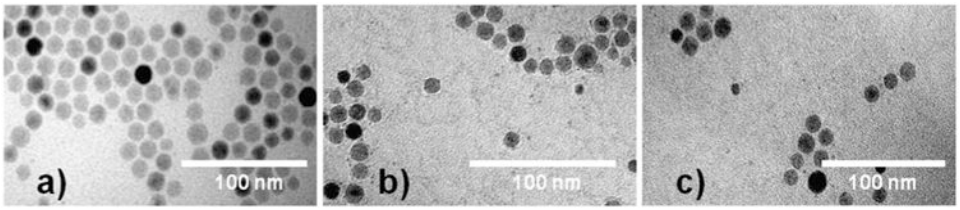

Fig. 2. TEM images of magnetic nanoparticles synthesized by the thermodecomposition method. Photos a, b, and c show images of magnetic nanoparticles coated with oleic acid, APS, and CMDx molecules, respectively

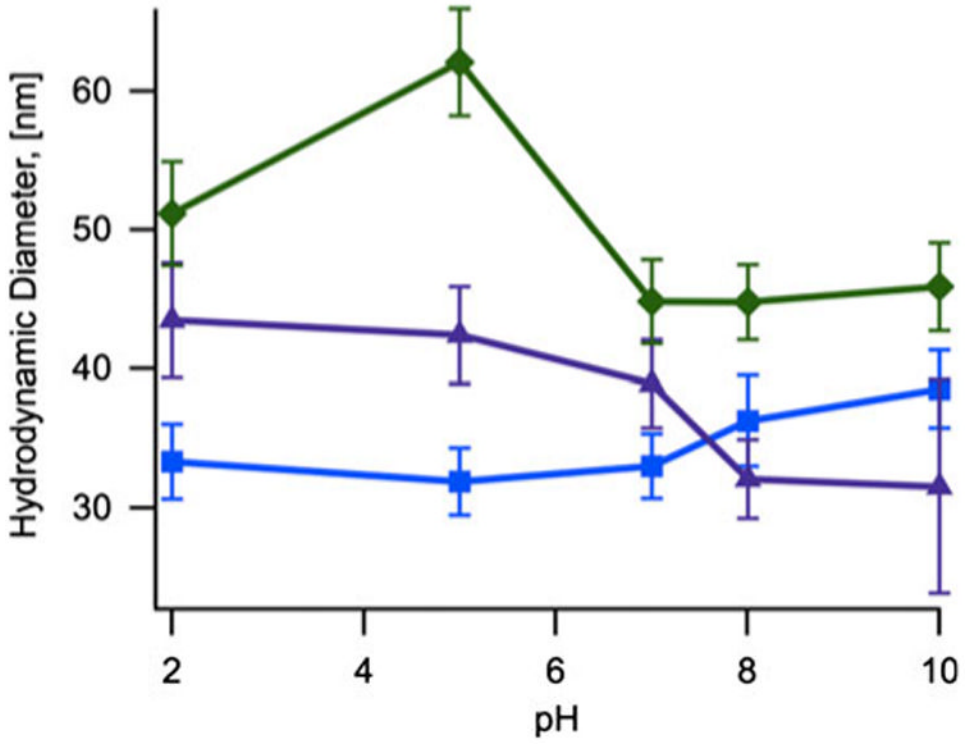

Fig. 3. Hydrodynamic diameter as a function of pH concentration for samples of magnetic nanoparticles coated with CMDx-a (*filled square*), CMDx-b (*filled triangle*), and CMDx-c (*filled diamond*)

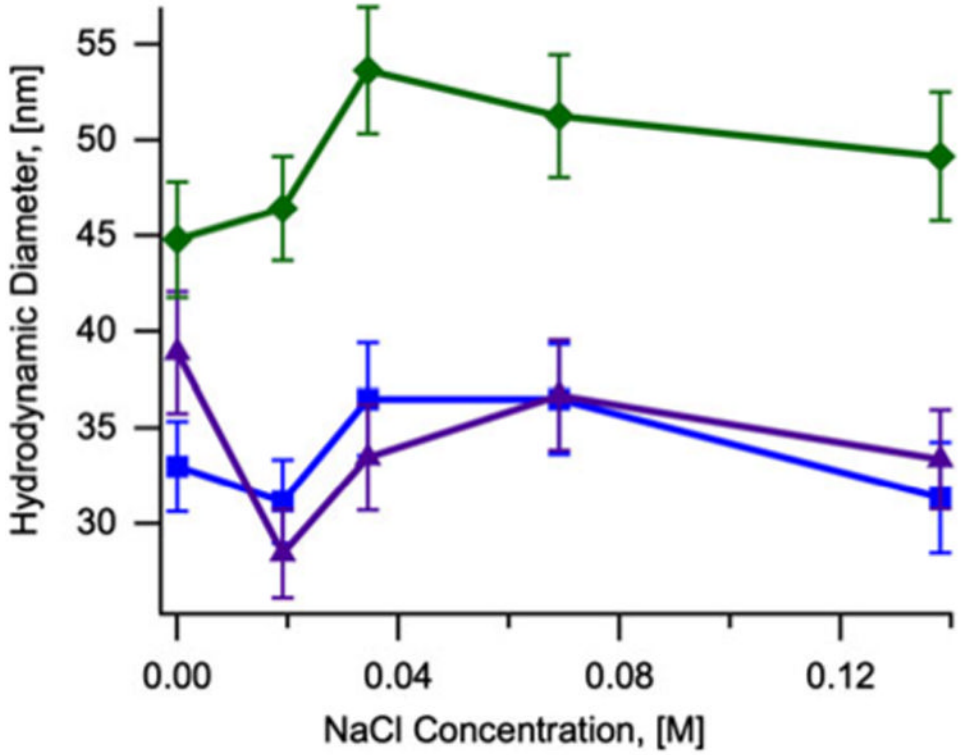

Fig. 4. Hydrodynamic diameter as a function of NaCl concentration for samples of magnetic nanoparticles coated with CMDx-a (*filled square*), CMDx-b (*filled triangle*), and CMDx-c (*filled diamond*)

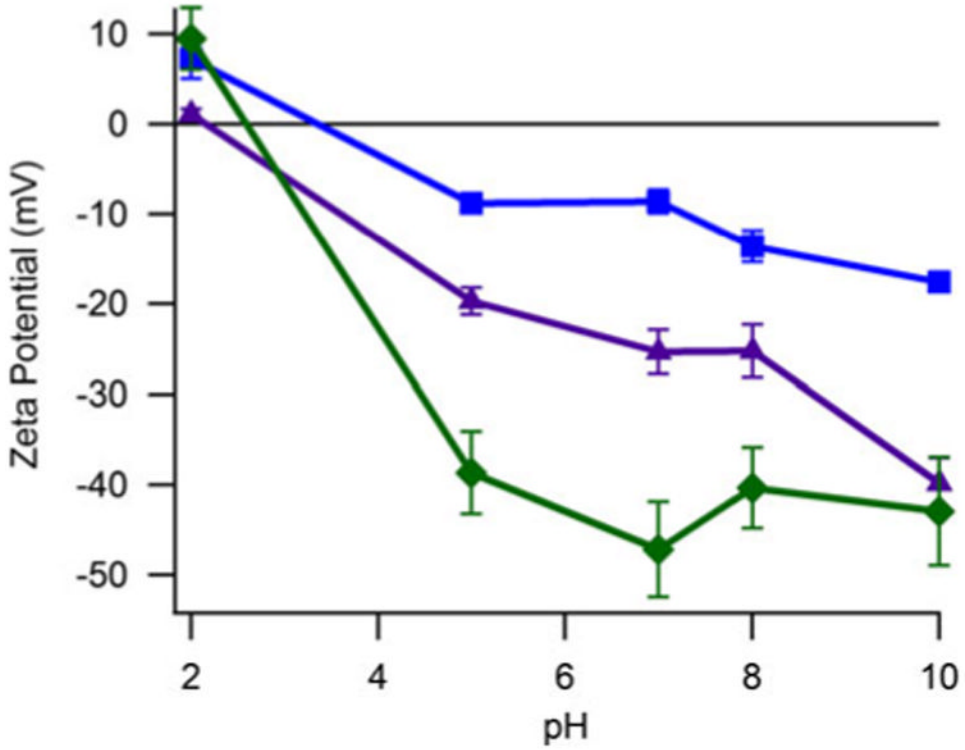

Fig. 5.

Zeta potential as function of pH for nanoparticles functionalized with APS and CMDx molecules and suspended in 1 mM KNO_3. *Filled Squares* illustrate CMDx-a-coated magnetic nanoparticles. *Filled triangles* show magnetic nanoparticles functionalized with CMDx-b molecules. *Filled diamonds* represent CMDx-c-coated magnetic nanoparticles

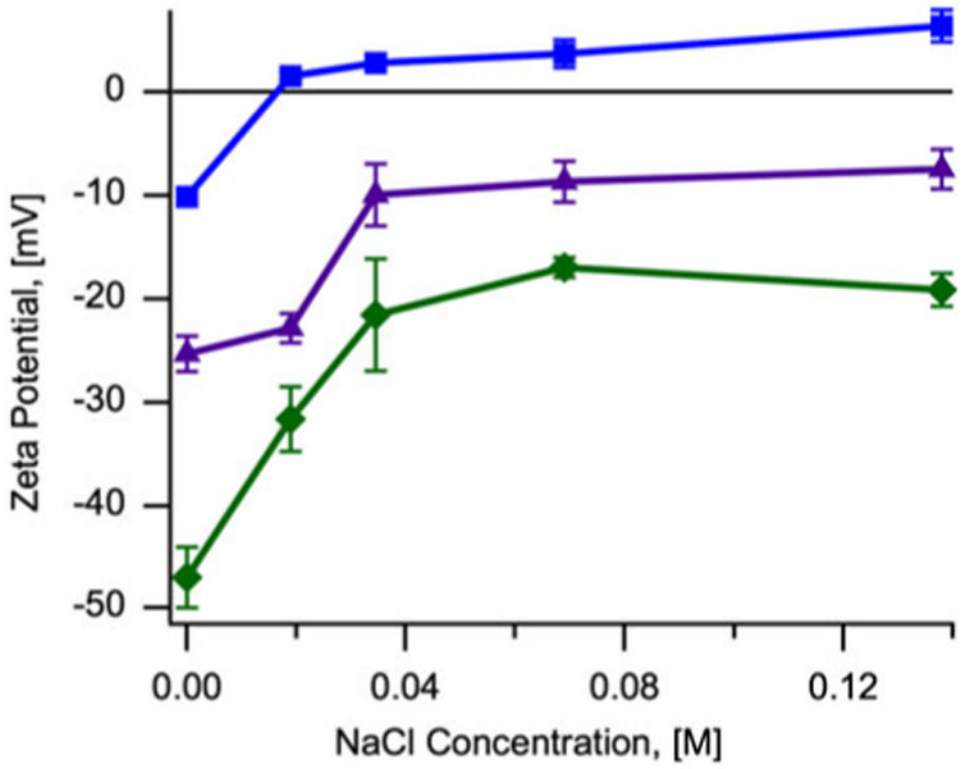

Fig. 6.

Variation of zeta potential as a function of NaCl concentration for magnetic nanoparticles functionalized with carboxymethyl-substituted dextran. *Filled Squares* illustrate CMDx-a-coated magnetic nanoparticles. *Filled triangles* show magnetic nanoparticles functionalized with CMDx-b molecules. *Filled diamonds* represent CMDx-c-coated magnetic nanoparticles

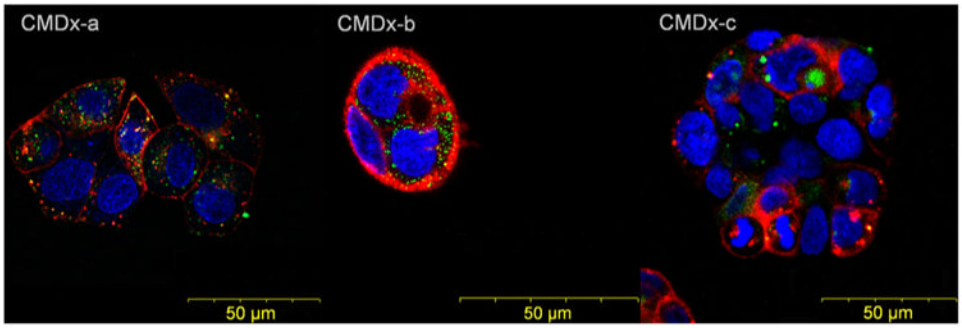

Fig. 7. Visualization of IO-CMDx nanoparticle uptake in CaCo-2 cells after 48 h of contact time

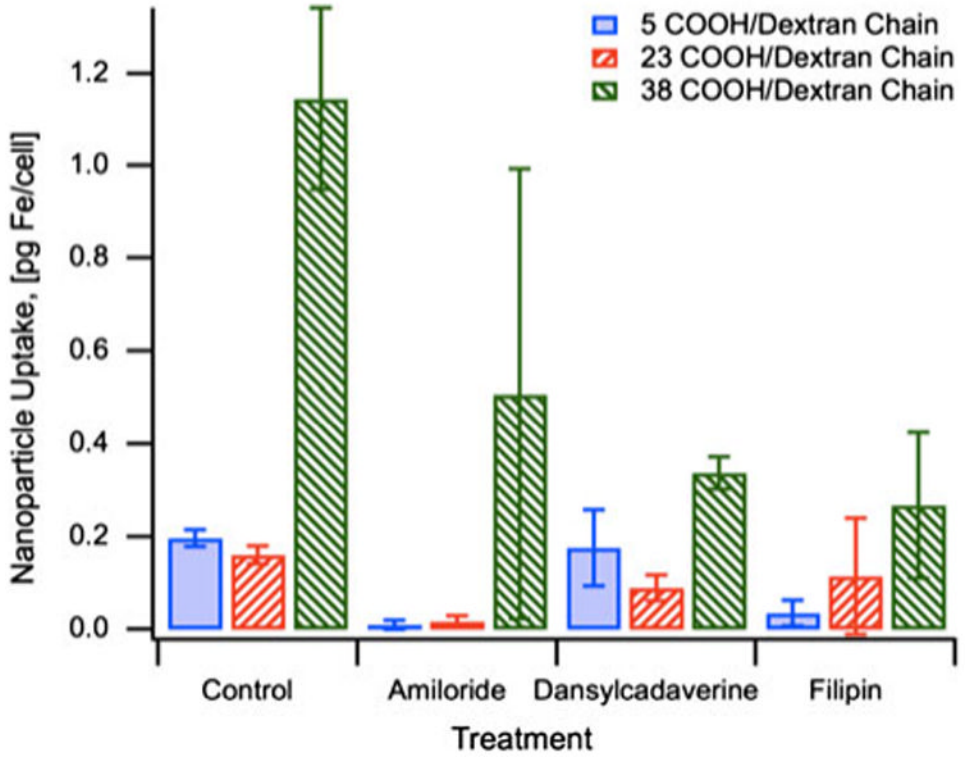

Fig. 8. Uptake of magnetic nanoparticles functionalized with carboxymethyl-substituted dextran and effect of uptake pathway inhibitors

Table 1

Characterization of carboxymethyl-substituted dextrans by acidimetric titration

Sample	DS	−COOH per chain
CMDx-a	0.08	5
CMDx-b	0.38	23
CMDx-c	0.61	38